

*High-precision measurements of the co-polar correlation coefficient: non-Gaussian errors and retrieval of the dispersion parameter  $\mu$  in rainfall*

Article

Accepted Version

Keat, W. J., Westbrook, C. D. and Illingworth, A. J. (2016) High-precision measurements of the co-polar correlation coefficient: non-Gaussian errors and retrieval of the dispersion parameter  $\mu$  in rainfall. *Journal of Applied Meteorology and Climatology*, 55 (7). pp. 1615-1632. ISSN 1558-8432 doi: <https://doi.org/10.1175/JAMC-D-15-0272.1> Available at <http://centaur.reading.ac.uk/62399/>

It is advisable to refer to the publisher's version if you intend to cite from the work. See [Guidance on citing](#).

To link to this article DOI: <http://dx.doi.org/10.1175/JAMC-D-15-0272.1>

Publisher: American Meteorological Society

All outputs in CentAUR are protected by Intellectual Property Rights law, including copyright law. Copyright and IPR is retained by the creators or other copyright holders. Terms and conditions for use of this material are defined in the [End User Agreement](#).

[www.reading.ac.uk/centaur](http://www.reading.ac.uk/centaur)

## **CentAUR**

Central Archive at the University of Reading

Reading's research outputs online

1 **High-Precision Measurements of the Co-Polar Correlation**

2 **Coefficient: Non-Gaussian Errors and Retrieval of the Dispersion**

3 **Parameter  $\mu$  in Rainfall**

4 **W. J. KEAT, \* C. D. WESTBROOK, AND A. J. ILLINGWORTH**

*Department of Meteorology, University of Reading, UK*

---

\* *Corresponding author address:* W. J. Keat, Department of Meteorology, University of Reading, Earley Gate, PO Box 243, Reading, RG6 6BB.

E-mail: w.j.keat@pgr.reading.ac.uk

5 ABSTRACT

6 The co-polar correlation coefficient ( $\rho_{hv}$ ) has many applications, including hydrometeor clas-  
7 sification, ground clutter and melting layer identification, interpretation of ice microphysics  
8 and the retrieval of rain drop size distributions (DSDs). However, we currently lack the  
9 quantitative error estimates that are necessary if these applications are to be fully exploited.  
10 Previous error estimates of  $\rho_{hv}$  rely on knowledge of the unknown ‘true’  $\rho_{hv}$  and implicitly  
11 assume a Gaussian probability distribution function of  $\rho_{hv}$  samples. We show that fre-  
12 quency distributions of  $\rho_{hv}$  estimates are in fact highly negatively skewed. A new variable:  
13  $L = -\log_{10}(1 - \rho_{hv})$  is defined, which does have Gaussian error statistics, and a standard  
14 deviation depending only on the number of independent radar pulses. This is verified using  
15 observations of spherical drizzle drops, allowing, for the first time, the construction of rigor-  
16 ous confidence intervals in estimates of  $\rho_{hv}$ . In addition, we demonstrate how the imperfect  
17 co-location of the horizontal and vertical polarisation sample volumes may be accounted for.

18 The possibility of using  $L$  to estimate the dispersion parameter ( $\mu$ ) in the gamma drop  
19 size distribution is investigated. We find that including drop oscillations is essential for  
20 this application, otherwise there could be biases in retrieved  $\mu$  of up to  $\approx 8$ . Preliminary  
21 results in rainfall are presented. In a convective rain case study, our estimates show  $\mu$  to  
22 be substantially larger than 0 (an exponential DSD). In this particular rain event, rain rate  
23 would be overestimated by up to 50% if a simple exponential DSD is assumed.

# 24 1. Introduction

25 The co-polar correlation coefficient,  $\rho_{hv}$ , between horizontal ( $H$ ) and vertical ( $V$ ) polari-  
26 sation radar signals is a measure of the variety of hydrometeor shapes in a pulse volume. It is  
27 therefore useful for applications such as identifying the melting layer (Caylor and Illingworth  
28 1989; Brandes and Ikeda 2004; Tabary et al. 2006; Giangrande et al. 2008), ground clutter  
29 (e.g. Tang et al. 2014), rain-hail mixtures (Balakrishnan and Zrnic 1990) and interpreting  
30 polarimetric signatures in ice (e.g. Andrić et al. 2013), and potentially the retrieval of  
31 the drop size distribution (DSD). The standard deviations of differential reflectivity ( $Z_{DR}$ )  
32 and differential phase shift ( $\phi_{dp}$ ) are both functions of  $\rho_{hv}$  (Bringi and Chandrasekar 2001).  
33 Therefore,  $\rho_{hv}$  dictates both the quality of dual polarisation measurements and their weight-  
34 ing in hydrometeor classification schemes (Park et al. 2009). In rainfall,  $\rho_{hv}$  is typically  
35 0.98—1. Giangrande et al. (2008) use data where  $\rho_{hv} < 0.97$  to identify the melting layer.  
36 For hail,  $\rho_{hv}$  can be much lower due to the effects of Mie scattering. At present, quantita-  
37 tive use of  $\rho_{hv}$  is hampered by a lack of rigorous confidence intervals accompanying the  $\rho_{hv}$   
38 estimates. Error estimates are available adopting an empirical approach (Illingworth and  
39 Caylor 1991) or a linear perturbation technique (Liu et al. 1994; Torlaschi and Gingras 2003),  
40 both of which implicitly assume a Gaussian probability distribution for the  $\rho_{hv}$  samples. We  
41 will show that the distribution of  $\rho_{hv}$  samples is in fact non-Gaussian and highly negatively  
42 skewed.

43 Natural rain drop size distributions can be described by a gamma distribution (Ulbrich  
44 1983):

$$N(D) = N_0 D^\mu \exp \left[ -\frac{(3.67 + \mu)}{D_0} D \right] \quad (1)$$

45 where  $D$  is the equivalent spherical drop diameter,  $N_0$  is the intercept parameter,  $D_0$  is the  
46 median volume drop diameter and  $\mu$  is the dispersion parameter (a measure of the drop size  
47 spectrum shape). If  $\mu = 0$ , by exploiting the relationship between drop diameter and drop

48 axis ratio,  $D_0$  can be estimated using  $Z_{DR}$  (Seliga and Bringi 1976). Higher  $\mu$  correspond  
49 to more monodisperse drop size distributions. Since  $\rho_{hv}$  is sensitive to variations in drop  
50 shape, it can in principle be used to estimate  $\mu$  (Jameson 1987), knowledge of which could  
51 improve dual polarisation and dual frequency (e.g. the Global Precipitation Measurement  
52 satellite) rain rate estimates. Figure 1 shows rain rate ( $R$ ) per unit radar reflectivity ( $Z$ ) as  
53 a function of  $Z_{DR}$  for simulated Gamma distributions with  $\mu = -1, 0, 2, 4, 8, 12$  and  $16$ . The  
54 rain rate is sensitive to variability in the shape of the drop size spectrum; uncertainty in  $\mu$   
55 alone could introduce an error in the retrieved rain rate of up to 2.5 dB (almost a factor of  
56 2) for a given pair of  $Z$  and  $Z_{DR}$  observations.

57 It is difficult to obtain reliable estimates of  $\mu$  from observations. Disdrometers suffer from  
58 undersampling of large drops, which cause  $\mu$  values that are derived from the 3<sup>rd</sup>, 4<sup>th</sup> and 6<sup>th</sup>  
59 moments of the drop size distribution to be biased high (Johnson et al. 2014). Furthermore,  
60 disdrometers also undercount the number of drops  $< 0.5$  mm (Tokay et al. 2001), which can  
61 also introduce a bias in estimates of  $\mu$ . Estimating DSD parameters using radar is therefore  
62 preferable, due to the very large number of drops being sampled. Wilson et al. (1997)  
63 made radar observations dwelling in rain at elevation angles above  $20^\circ$  and report that the  
64 difference in the mean Doppler velocity at  $H$  and  $V$  polarisations provides an estimate of  $\mu$ ,  
65 which were in the range of 1 to 11, and, once  $Z_{DR}$  exceeded 0.5 dB, all the values were above  
66 4. Doppler spectra of rain at vertical incidence with multiple wavelength radars, including  
67 wind profiler frequencies that respond to the clear air motion have been utilised to estimate  
68  $\mu$  (Williams 2002; Schafer et al. 2002). These experiments find  $\mu$  ranges between 0 and 18,  
69 but is typically 0—6. Unal (2015) fits observed Doppler spectra to theoretical drop spectra  
70 at S-band, and retrieves  $\mu$  in the range of -1—5. The disadvantage of these techniques is that  
71 they use high elevation angles; for operational monitoring of surface rainfall, measurements  
72 at low elevation angles are preferable. This motivates the use of  $\rho_{hv}$  to derive  $\mu$  in rainfall.  
73 Illingworth and Caylor (1991) and Thurai et al. (2008) inferred  $\mu$  from the decrease in  
74  $\rho_{hv}$  as  $Z_{DR}$  increases. The difficulty here is that any mis-matches in the  $H$  and  $V$  beams

75 will introduce an uncorrelated noise component, so that even for perfectly spherical drizzle  
76 droplets, where the “true”  $\rho_{hv}$  is unity, the radar will always detect a value less than one (we  
77 will call this maximum obtainable level of  $\rho_{hv}$  “ $f_{hv}^{max}$ ”, see Section 5). From measurements in  
78 rain at short range, Illingworth and Caylor (1991) inferred  $\mu$  values, which if corrected with  
79 an estimate of  $f_{hv}^{max}$  were in the range 0–2, but even for long dwells the estimated errors  
80 in  $\mu$  were quite large. Thurai et al. (2008) analysed  $\rho_{hv}$  measurements from an operational  
81 radar and obtained estimates of  $\mu$  in the range of 1–3, however their approach relies on  
82 empirically derived relationships between  $\rho_{hv}$  and DSD widths from 2 dimensional video  
83 disdrometer (2DVD) measurements. Furthermore, the technique is only valid for intense  
84 rain ( $Z_{DR} \geq 2$  dB and  $\rho_{hv} < 0.98$ ).

85 The aim of this paper is to define a new variable,  $L = -\log_{10}(1 - \rho_{hv})$ , that has Gaussian  
86 error statistics with a width predictable from the number of independent radar pulses. This  
87 can be readily estimated by using the observed Doppler spectral width ( $\sigma_v$ ). We will then  
88 present measurements of  $L$  in rainfall as a function of  $Z_{DR}$ , and retrieve estimates of  $\mu$  by  
89 comparing these with predicted  $L$  and  $Z_{DR}$  for various three-parameter gamma distributions.  
90 The possibility of using this technique to retrieve  $\mu$  using operational radars is then discussed.

## 91 2. The Co-Polar Correlation Coefficient ( $\rho_{hv}$ )

92  $\rho_{hv}$  is defined as (Doviak and Zrnic 2006):

$$\rho_{hv} = \frac{\langle S_{VV} S_{HH}^* \rangle}{\sqrt{\langle |S_{HH}|^2 \rangle \langle |S_{VV}|^2 \rangle}} \quad (2)$$

93 where  $\langle S_{HH} \rangle$  and  $\langle S_{VV} \rangle$  are the co-polar elements of the backscattering matrix averaged  
94 over an ensemble of scatterers for the  $H$  and  $V$  polarisations respectively, and \* indicates the  
95 complex conjugate. It can be estimated by correlating successive power or complex ( $I$  and  
96  $Q$ ) measurements. Examples of power time-series in (a) drizzle and (b) heavier rainfall from

97 the 3 GHz Chilbolton Advanced Meteorological Radar (CAMRa) are shown in figure 2. The  
 98 radar is a coherent-on-receive magnetron system, transmitting and receiving alternate  $H$  and  
 99  $V$  polarised pulses with a pulse repetition frequency (PRF) of 610 Hz. A cubic polynomial  
 100 interpolation is used to estimate the  $H$  power at the  $V$  pulse timing and the  $V$  power at the  
 101  $H$  pulse timing. Its narrow one-way half power beamwidth ( $0.28^\circ$ ) makes it capable of very  
 102 high resolution measurements. The full capabilities of this radar are discussed in Goddard  
 103 et al. (1994). The observed fluctuating signals in Figure 2 are caused by the superposition  
 104 of the backscattered waves from each drop in the sample volume; the rate of fluctuation  
 105 is determined by the Doppler spectral width. For drizzle, since the drops are spherical,  
 106  $Z_{DR} = 0$  dB, and the  $H$  and  $V$  signals are almost perfectly correlated:  $\rho_{hv} = 0.995$ . For  
 107 heavier rainfall, a systematically lower  $V$  power is received ( $Z_{DR} = 1.1$  dB), and the signals  
 108 are visibly less correlated ( $\rho_{hv} = 0.987$ ), due to the broader axis ratio distributions in the  
 109 sample volume.

110 These estimates of  $\rho_{hv}$  are derived from a finite number of reshufflings, and therefore  
 111 there is some uncertainty in them. In what follows, we quantify this uncertainty.

### 112 **3. Theoretical Measurement Error in Estimated Corre-** 113 **lation of Time-Series**

114 Figure 3a shows the distribution of estimates of the correlation coefficient,  $\hat{\rho}_{hv}$  (calculated  
 115 from a finite length time-series), as distinct from the “true” co-polar correlation coefficient,  
 116  $\overline{\rho_{hv}}$  (that would be measured for a time-series of infinite length). The data was collected  
 117 during a  $1.5^\circ$  elevation dwell in drizzle ( $Z_{DR} < 0.1$  dB), with very high SNR ( $> 40$  dB) on  
 118 6 February 2014. Each  $\hat{\rho}_{hv}$  is calculated from 64  $H$  and  $V$  pulse pairs (0.21s dwell) from a  
 119 single 75 m range gate with  $\sigma_v = 1.1 \pm 0.1$  ms<sup>-1</sup>. The distribution of  $\hat{\rho}_{hv}$  has a peak that is  
 120 close to  $\overline{\rho_{hv}}$  (which is  $< 1$ , see Section 5d), but exhibits a very long tail at lower  $\hat{\rho}_{hv}$ , while  
 121 there are no data with  $\hat{\rho}_{hv} > 1$ . Clearly, this distribution is not Gaussian and the negative



122 skewness will negatively bias the mean of many  $\rho_{hv}$  samples compared to the true value of  
 123  $\rho_{hv}$ .

124 Fisher (1915) states that sample correlation coefficients ( $\hat{\rho}$ ) of a “true” correlation coef-  
 125 ficient ( $\bar{\rho}$ ) calculated from a finite number of Gaussian random variables are skewed for  $\bar{\rho} \neq$   
 126 0. However, the variable:

$$\hat{F} = \frac{1}{2} \ln \left( \frac{1 + \hat{\rho}}{1 - \hat{\rho}} \right) \quad (3)$$

127 is Gaussian, with a mean of:

$$\bar{F} = \frac{1}{2} \ln \left( \frac{1 + \bar{\rho}}{1 - \bar{\rho}} \right) \quad (4)$$

128 and standard error of:

$$\sigma_F = \frac{1}{\sqrt{N - 3}} \quad (5)$$

129 where  $N$  is the number of independent samples used to calculate  $\hat{\rho}$ .

130 This is directly applicable to estimates of the radar co-polar correlation coefficient, by  
 131 realising that the  $I$  and  $Q$  samples that are used to estimate  $\rho_{hv}$  are Gaussian random  
 132 variables (Doviak and Zrnic 2006). Noting that  $\rho_{hv}$  in meteorological targets is always close  
 133 to unity so that fractional changes in  $(1 - \rho_{hv})$  are always much greater than  $(1 + \rho_{hv})$ ,  
 134 Equation 3 can be written as:

$$\hat{F} \approx \frac{1}{2} \ln 2 - \frac{\ln 10}{2} \log_{10}(1 - \rho_{hv}) \quad (6)$$

135 Since  $\hat{F}$  is normally distributed, the quantity:

$$\hat{L} = -\log_{10}(1 - \rho_{hv}) \quad (7)$$

136 is also normally distributed, with a mean:

$$\bar{L} = -\log_{10}(1 - \overline{\rho_{hv}}) \quad (8)$$

137 and standard deviation of:

$$\sigma_L = \frac{2}{\ln 10} \times \frac{1}{\sqrt{N_{IQ} - 3}} \quad (9)$$

138 for  $N_{IQ} \gg 3$ , where  $N_{IQ}$  is the number of independent  $I$  and  $Q$  samples used to calculate  
 139  $\hat{\rho}_{hv}$ . Despite having similar characteristics,  $L$  is preferred over the use of  $F$  as it has the  
 140 convenient property that  $\rho_{hv} = 0.9, 0.99$  and  $0.999$  correspond to  $L = 1, 2$  and  $3$  respectively  
 141 and therefore is more intuitive. Illingworth and Caylor (1991) plotted their  $\hat{\rho}_{hv}$  data as  
 142  $\log_{10}(1 - \hat{\rho}_{hv})$  and their histograms also appear Gaussian in shape. Figure 3b illustrates the  
 143 effect of the transform  $\hat{L} = -\log_{10}(1 - \hat{\rho}_{hv})$  on the distribution in Figure 3a. The histogram  
 144 is now symmetrical, and bell shaped. A Gaussian curve with an equal mean and standard  
 145 deviation to the  $\hat{L}$  PDF is overplotted and is an excellent fit to the data, showing that the  
 146 distributions are indeed Gaussian (and Quantile - Quantile plots, not shown here for brevity,  
 147 confirm this).

148 To determine the number of independent  $I$  and  $Q$  samples,  $N_{IQ}$ , we consider the auto-  
 149 correlation function for  $I$  and  $Q$  samples given by Doviak and Zrnic (2006):

$$R_{IQ}(nT_s) = \exp \left[ -8 \left( \frac{\pi \sigma_v n T_s}{\lambda} \right)^2 \right] \quad (10)$$

150 where  $T_s$  is the time spacing between pulses of the same polarisation and  $nT_s$  is the total  
 151 time lag. Following the definition of Papoulis (1965), the time to independence for  $I$  and  $Q$   
 152 samples for large  $N_{IQ}$  can be shown to be:

$$\tau_{IQ} = \frac{\lambda}{2\sqrt{2}\pi\sigma_v} \quad (11)$$

153 where  $\lambda$  is the radar wavelength and  $\sigma_v$  is the Doppler spectral width. This is a factor of  $\sqrt{2}$   
 154 smaller than the more often used time to independence for reflectivity samples. The number

155 of independent  $I$  and  $Q$  pulses per  $\rho_{hv}$  sample can therefore be estimated by:

$$N_{IQ} = \frac{T_{dwell}}{\tau_{IQ}} = \frac{2\sqrt{2\pi}\sigma_v T_{dwell}}{\lambda} \quad (12)$$

156 where  $T_{dwell}$  is the dwell time.

157 The result (Equation 9) is significant as it shows that a confidence interval for any  
 158 measurement of  $\rho_{hv}$  can be calculated solely in terms of the number of independent  $I$  and  
 159  $Q$  samples used to estimate it, which in turn can be readily estimated using the observed  
 160 Doppler spectral width and Equation 12. Furthermore, when multiple samples of  $\hat{L}$  are  
 161 averaged, no bias is introduced to estimates of  $\rho_{hv}$  because of the non-linear transform. We  
 162 expand this point in Section 4.

163 To estimate confidence intervals for measurements of  $\rho_{hv}$ , one must:

- 164 • Apply the transform  $\hat{L} = -\log_{10}(1 - \rho_{hv})$
- 165 • Calculate the standard deviation of  $\hat{L}$  using Equation 9.
- 166 • Apply the inverse transform  $1 - 10^{-(\hat{L} \pm \sigma_L)}$  to obtain upper and lower confidence intervals  
 167 (where  $\sigma_L$  will contain the true value 68% of the time and  $2\sigma_L$  98%).

168 More conveniently, one can simply transform  $\rho_{hv}$  data to  $\hat{L}$  and use this for any subsequent  
 169 analysis, with confidence intervals of  $\hat{L} \pm \sigma_L$ . This is the approach we follow in the rest  
 170 of this paper. Although we are focusing on data with very high signal-to-noise (SNR) in  
 171 this paper, the theory above should also be valid for weak SNR data, providing that noise  
 172 introduced is also Gaussian in the  $I$  and  $Q$  samples.

173 This theoretical prediction was tested by comparing estimates of  $\sigma_L$  using data collected  
 174 in homogeneous drizzle ( $Z_{DR} < 0.1$  dB) with very good signal-to-noise (SNR  $> 40$  dB).  
 175 In drizzle,  $\bar{L}$  is constant since the drops are spherical, and therefore any variation  $\sigma_L$  is  
 176 due to the finite  $N_{IQ}$ . Pulse-to-pulse  $H$  and  $V$  powers were recorded, and time series of  
 177 various lengths between 0.2—30 s were constructed from these data and used to compute

178 the corresponding  $N_{IQ}$  and  $L$  values. Data was binned by  $N_{IQ}$ , and the standard deviation,  
 179  $\sigma_L$ , were computed for each bin. Figure 4 shows how  $\sigma_L$  decreases as  $N_{IQ}$  is increased over  
 180 more than two orders of magnitude.  $\sigma_L$  is slightly overestimated for  $N_{IQ} \approx 10$ , and the data  
 181 is in excellent agreement to that predicted by Equation 9 for  $N_{IQ} > 30$ .

## 182 4. Comparison with Existing Error Statistics

183 We now compare these new error statistics with existing methods in the literature. From  
 184 observations of  $\rho_{hv}$  in rain, the bright-band and ice, Illingworth and Caylor (1991) derived  
 185 empirically the relationship between their mean  $\hat{\rho}_{hv}$  estimates and their standard deviation:

$$\sigma_{\rho_{hv}}^{IC} \simeq \frac{1.25(1 - \hat{\rho}_{hv})}{\sqrt{n}} \quad (13)$$

186 where  $n$  is the number of 0.2 s time-series they used to estimate the mean  $\rho_{hv}$ . Using a linear  
 187 perturbation technique, Torlaschi and Gingras (2003) derive the following equation for the  
 188 standard deviation on a  $\rho_{hv}$  measurement:

$$\sigma_{\rho_{hv}}^{TG} = \frac{1 - \bar{\rho}_{hv}^2}{\sqrt{2N_I}} \quad (14)$$

189 where  $N_I$  is the number of independent radar reflectivity samples used in its estimation. Note  
 190 that  $\bar{\rho}_{hv}$  in Equation 14 is the “true” correlation coefficient one is attempting to measure  
 191 (rather than the measured value,  $\hat{\rho}_{hv}$ ). This equation represents the standard deviation  
 192 for infinite SNR conditions, and is valid for simultaneous or accurately interpolated  $H$  and  
 193  $V$  sampling. Neither of these techniques are ideal, relying on either knowing a-priori the  
 194 true correlation coefficient one is attempting to measure (Torlaschi and Gingras 2003), or a  
 195 number of time-series (Illingworth and Caylor 1991), not the number of independent pulses.  
 196 It is not possible to compare the method of Illingworth and Caylor (1991) with our proposed  
 197 method as  $\sigma_v$  for their data is unknown, and therefore the number of independent pulses in  
 198 their time-series cannot be quantified. Figure 5a shows the errors on  $\hat{\rho}_{hv}$  calculated using our

199 new method compared to those calculated using the linear perturbation method of Torlaschi  
 200 and Gingras (2003) as a function of  $N_{IQ}$  in rain ( $\overline{\rho_{hv}} = 0.98$ ). The magnitudes of the upper  
 201 confidence bounds are largely similar, however, for all  $N_{IQ}$  the lower confidence interval is  
 202 higher for Torlaschi and Gingras (2003) (i.e smaller deviations from  $\overline{\rho_{hv}}$  are predicted), due  
 203 to the asymmetric nature of the new confidence intervals on  $\rho_{hv}$ . The largest difference is for  
 204 small  $N_{IQ}$ . As  $N_{IQ}$  increases, both the upper and lower confidence intervals for each method  
 205 converge. Although Figure 5a serves as a useful illustration of the difference between the  
 206 methods, they are not strictly comparable in practice: the error calculation of Torlaschi and  
 207 Gingras (2003) relies on knowledge of  $\overline{\rho_{hv}}$  which in reality is unknown. Conversely, the new  
 208 method requires no a-priori knowledge of  $\overline{\rho_{hv}}$ , and so is of much greater practical use.

209 Figure 5b illustrates the theoretical bias introduced by averaging many short samples of  
 210  $\rho_{hv}$ , rather than  $\hat{L}$ , in rain ( $\overline{\rho_{hv}} = 0.98$ ). This bias is significant for small  $N_{IQ}$ . For example,  
 211 when  $N_{IQ} = 10$ , the bias on  $\hat{L}$  is 0.1, which is significant for the purpose of estimating  $\mu$  in  
 212 rainfall; this bias in  $L$  could lead to an underestimate of  $\mu$  of  $\approx 8$  at  $Z_{DR} = 2$  dB (see figure  
 213 8). It is not important whether spatial or temporal averaging is used to increase the number  
 214 of independent  $I$  and  $Q$  samples, as long as  $\overline{\rho_{hv}}$  does not vary substantially over the scales  
 215 considered.

216 In summary, confidence intervals that rely on the linear perturbation method overestimate  
 217 the precision of  $\rho_{hv}$  measurements, and require knowledge of the “true”  $\rho_{hv}$  one is attempting  
 218 to measure. Fundamentally, failure to use the transform  $L$  when averaging short time-  
 219 series will lead to significant biases in correlation coefficient estimates. This is particularly  
 220 important for operational  $\rho_{hv}$  applications that typically use very short dwell times (discussed  
 221 in Section 8a), and would lead to a significant bias in retrievals of  $\mu$  in rain.

## 222 5. Practical measurement of $\rho_{hv}$

223 To fully exploit our new error estimates, and retrieve rain DSDs, some practical consid-  
224 erations for the measurement of  $\rho_{hv}$  must first be considered.

### 225 a. *Effect of alternate sampling*

226 When estimating the correlation coefficient, the non-simultaneous transmission and re-  
227 ception of  $H$  and  $V$  pulses must be accounted for. Assuming a Gaussian autocorrelation  
228 function to correct for this staggered sampling (Sachidananda and Zrnic 1989) can lead to  
229 unphysical samples where  $\hat{\rho}_{hv} > 1$  (Illingworth and Caylor 1991). In our analysis, we employ  
230 a cubic polynomial interpolation to obtain  $H$  and  $V$  power estimates at the intermediate  
231 sampling intervals (Caylor 1989), which is very effective. We find that the interpolation  
232 scheme works well: for drizzle with  $\bar{L} = 2.4$ , we observe that average values of  $\hat{L}$ , binned  
233 by  $\sigma_v$ , are constant to within  $\pm 0.02$  as  $\sigma_v$  varies between 0.1—2 ms<sup>-1</sup>. This is evidence  
234 of successful interpolation, since there is no systematic trend to lower  $L$  values at higher  
235 spectral widths.

### 236 b. *Signal-to-noise ratio*

237 The addition of noise to the received signals acts to reduce the correlation between  $H$   
238 and  $V$  time-series. The reduction factor,  $f$ , has been shown (Bringi et al. 1983) to vary  
239 predictably as:

$$f = \frac{1}{\left(1 + \frac{1}{SNR_H}\right)^{\frac{1}{2}} \left(1 + \frac{1}{SNR_V}\right)^{\frac{1}{2}}} \quad (15)$$

240 for simultaneous (or accurately interpolated)  $H$  and  $V$  sampling, where  $SNR_H$  and  $SNR_V$   
241 are the signal-to-noise ratios for the  $H$  and  $V$  polarisations respectively. This was verified by

242 Illingworth and Caylor (1991) with measurements of  $\rho_{hv}$  in drizzle. Whilst it is in principle  
 243 possible to correct for the presence of noise using this equation, due to the high degree of  
 244 precision required in this work, only data with SNR  $> 34$  dB are included in our analysis,  
 245 which corresponds to a maximum achievable  $\rho_{hv}$  measurement of 0.9996. However, instru-  
 246 mental effects (described in Section d below) will have the same effect of adding uncorrelated  
 247 noise, and so in practice this maximum value is never reached.

248 *c. Effect of phase error*

249 To avoid a bias in  $\hat{\rho}_{hv}$  due to random phase error from our magnetron system (Liu et al.  
 250 1994), we cross correlate the power of the received echoes as opposed to the complex  $I$  and  
 251  $Q$  signals, and take the square root, following Illingworth and Caylor (1991).

252 *d. Instrumental effects*

253 Even in drizzle with very high SNR, antenna imperfections and other effects such as  
 254 irregular magnetron pulse timing and pulse shape reproducibility will cause measured  $\rho_{hv}$  to  
 255 always be  $< 1$  (Illingworth and Caylor 1991; Liu et al. 1994) as effectively they cause the  $H$   
 256 and  $V$  pulses to sample slightly different volumes. Here, we propose a method to quantify  
 257 and account for this bias, analogous to the SNR factor (Equation 15) suggested by Bringi  
 258 et al. (1983). We consider the  $H$  and  $V$  echoes to consist of two parts: a common sample  
 259 volume, and parts of each sample volume which are unique to a particular polarisation. By  
 260 treating the former as “signal” and the latter as unwanted “noise”, we obtain an equation  
 261 similar to Equation 15. Full details are provided in the appendix. The practical upshot  
 262 is that the measured  $\rho_{hv}$  is the “true”  $\rho_{hv}$  multiplied by some dimensionless factor,  $f_{hv}^{max}$ ,  
 263 relating to how well matched the  $H$  and  $V$  sample volumes are. For spherical drops,  $\overline{\rho_{hv}}$   
 264 should be unity. The estimates of  $\overline{\rho_{hv}}$  for all such data should therefore be equal to  $f_{hv}^{max}$ .  
 265 When comparing observations with simulated  $\rho_{hv}$ , we multiply each of the predicted values

266 by  $f_{hv}^{max}$  so that they are directly comparable to the observations.  $\rho_{hv}$  has been measured  
 267 in drizzle ( $Z_{DR} < 0.1$  dB) for a large number of samples on several days. Typically,  $f_{hv}^{max}$  is  
 268  $\approx 0.996$ , but varies by  $\pm 0.001$  from day to day, which we suggest is the result of slightly  
 269 irregular magnetron pulse timing and shape reproducibility for the CAMRa system, which  
 270 may be temperature dependent. For this reason,  $f_{hv}^{max}$  has been determined individually for  
 271 each case.

## 272 **6. Using $L$ and $Z_{DR}$ to Estimate $\mu$ in Rainfall**

273 We now attempt to use our high-precision measurements of  $L$  to retrieve  $\mu$  estimates  
 274 in rainfall. The independence of  $(D_0, \mu)$  and  $(L, Z_{DR})$  on the drop number concentration  
 275 means that a single  $L$  and  $Z_{DR}$  observation pair corresponds to a unique  $D_0$  and  $\mu$  value. In  
 276 order to forward model  $L$  and  $Z_{DR}$  for various gamma distributions, we must first assume  
 277 an appropriate drop shape model.

### 278 *a. Mean Drop Shapes*

279 There are numerous drop shape parameterisations in the literature. Here, we examine  
 280 drop axis ratios and diameters from the recent experiments of Thurai and Bringi (2005),  
 281 Szakáll et al. (2008) and the 4<sup>th</sup> order polynomial fit to many experiments given by Brandes  
 282 et al. (2002). Figure 6a shows the mean axis ratio as a function of drop diameter, for each  
 283 of these models. The Thurai and Bringi (2005) data suggests that mean drop shapes are  
 284 slightly prolate for  $D < 1$  mm, although it is in the margin of measurement error that the  
 285 drops are spherical (Beard et al. 2010). Since it is known that drops become spherical as  
 286 their diameter tends to 0 mm due to surface tension, our fit to the data is adapted so that  
 287 drops  $< 1$  mm are precisely spherical.

288 To choose the best mean drop shape model, a 5 hour dwell was made with CAMRa at a  
 289  $1.5^\circ$  elevation angle over a nearby Joss-Waldvogel RD-80 impact disdrometer (approximately



290 7 km away) in a frontal rain band on 25 April 2014. The disdrometer measures drop sizes in  
 291 127 size bins from 0.3 to 5.0 mm. The instrument is regularly calibrated by the manufacturer  
 292 and rain rate estimated with this instrument agrees very well with that from a co-located  
 293 rain gauge. Radar measurements of  $Z_{DR}$  are calibrated regularly (to within  $\pm 0.1$  dB) by  
 294 making observations of drizzle (low  $Z$ ), which we know to have a  $Z_{DR}$  value of 0 dB. The  
 295 range resolution of the radar measurements is 75 m, and averaged to 30 s to match the  
 296 integration time used by the disdrometer to estimate the DSD parameters. At this elevation  
 297 angle, the radar was sampling rain at a height of 183m above the disdrometer. Figures  
 298 6b—d show the observed radar measurement from the closest gate to the disdrometer, and  
 299 the corresponding disdrometer  $Z_{DR}$  values calculated using the Thurai and Bringi (2005),  
 300 Szakáll et al. (2008) and Brandes et al. (2002) drop shape models respectively. The Szakáll  
 301 et al. (2008) axis ratios are systematically smaller compared to both of the other models for  
 302 almost all  $D$ . Using this model makes the disdrometer estimates of  $Z_{DR}$  always larger than  
 303 the radar estimates. Thurai and Bringi (2005) and Brandes et al. (2002) agree for  $D = 2$ — $7$   
 304 mm, after which the axis ratios of Thurai and Bringi (2005) are closer to those of Szakáll  
 305 et al. (2008). Therefore, radar and disdrometer  $Z_{DR}$  for the Thurai and Bringi (2005) and  
 306 Brandes et al. (2002) models largely agree, apart from  $Z_{DR} \lesssim 0.4$  dB. The largest differences  
 307 between these models occurs for  $D < 2$  mm. Here, Szakáll et al. (2008) and Brandes et al.  
 308 (2002) predict more oblate drops than Thurai and Bringi (2005).

309 The Szakáll et al. (2008) model produces the largest radar-disdrometer overall bias of  
 310  $\approx 0.23$  dB. The biases from Brandes et al. (2002) for  $Z_{DR}$  bins of 0.2, 0.4 and 0.6 dB ( $\pm$   
 311 0.1 dB bin width) are 0.09, 0.16 and 0.13 dB respectively. For Thurai and Bringi (2005),  
 312 they are only 0.04, 0.08 and 0.09 dB respectively, and are very similar to Brandes et al.  
 313 (2002) at higher  $Z_{DR}$ . These reduced biases at low  $Z_{DR}$  suggest that the experimental  
 314 results of Thurai and Bringi (2005) best represent natural raindrop shapes. We therefore  
 315 chose this model in our analysis. It is unclear why the very small residual difference between  
 316 radar and disdrometer estimates of  $Z_{DR}$  using the Thurai and Bringi (2005) shape model is

317 observed. Some possible explanations are that the radar calibration is slightly out causing a  
318 systematic underestimation, the small sampling volume of the disdrometer could be biasing  
319  $Z_{DR}$ , or there could be residual error in the mean drop shape model. However, this very  
320 small difference is unimportant for retrievals that follow.

### 321 *b. Drop Oscillations*

322 Drop oscillations increase the variety of shapes within a radar pulse volume at any given  
323 time. This means that the  $\bar{L}$  we are attempting to estimate will be lower than that predicted  
324 by modelling only the mean drop axis ratios for drops of a given size. In order to account  
325 for this, we must parameterise these drop oscillations. In the Thurai and Bringi (2005)  
326 experiment, artificial rain drops were created from a hose and allowed to fall 80 m from  
327 a bridge before drop axis ratio and counts were measured with a 2D video disdrometer  
328 (2DVD) on the valley floor. This fall distance is more than sufficient to allow the drops to  
329 achieve steady state oscillations, and so the standard deviations of axis ratios measured in  
330 this experiment are interpreted as drop oscillation amplitudes. However, the large standard  
331 deviations of the axis ratios for  $D < 2$  mm are likely artificial, caused by the finite resolution  
332 of the 2DVD instrument (Beard et al. 2010). Since drop oscillations are thought to originate  
333 from vortex shedding (Beard et al. 2010) which increases as a function of drop size, the  
334 magnitude of oscillations should decrease eventually to zero as the drop diameter tends to  
335 0 mm. Beard and Kubesh (1991) suggest that resonant drop oscillations occur for drop  
336 sizes between 1.1 and 1.6 mm, however more recent measurements from the Mainz wind  
337 tunnel show that amplitudes of the axis ratios for these drop sizes were less than 0.025  
338 (Szakáll et al. 2010). For this reason, the polynomial fit to oscillation amplitude data from  
339 the Mainz wind tunnel (Szakáll et al. 2010) is used for  $D < 2$  mm, which has the desired  
340 reduction in oscillation amplitude for small drops <sup>1</sup>. For  $D > 2$  mm, we revert to the more

---

<sup>1</sup>Equation 1 in Szakáll et al. (2010) does not agree with the fit in Figure 3 (black line). By digitising the Mainz wind tunnel data, we calculate that Equation 1 should in fact be  $1.8 \times 10^{-3} D_0^2 + 1.07 \times 10^{-2} D_0$

341 statistically robust drop oscillations from Thurai and Bringi (2005). Since the oscillations  
 342 are aerodynamically induced, with an amplitude only a function of the drop size, they should  
 343 not vary with environmental conditions. In our analysis, the oscillations were included by  
 344 integrating over Gaussian PDFs of axis ratios (Thurai and Bringi 2005) in our Gans theory  
 345 computations. Figure 7 shows the effect of oscillations on computed  $L$  and  $Z_{DR}$  for values  
 346 of  $\mu = -1$  (black lines),  $\mu = 16$  (grey lines). Including drop oscillations for the purpose of  
 347 estimating  $\mu$  becomes increasingly important with increasing  $Z_{DR}$ ; the difference between  $L$   
 348 at  $\mu = 16$  computed with and without oscillations is as large as an equivalent change in  $\mu$  of  
 349  $\approx 8$ . We find that the modification of the oscillation magnitudes for drop diameters  $< 2$  mm  
 350 has a relatively small impact ( $< 0.01$ ) on predicted  $L$  for  $Z_{DR}$  larger than 0.8 dB where we  
 351 attempt retrievals of  $\mu$ . However, we find that the use of Szakáll et al. (2010) oscillations for  
 352 all drop diameters has a large impact on predicted  $L$  values (for  $\mu = -1$ ,  $L$  is  $\approx 0.1$  lower).  
 353 This is potentially important for retrievals of  $\mu$ .

354 Comparatively large amplitude (but short lived, lasting less than  $\approx 0.4$  s) collision in-  
 355 duced oscillations can also occur (Szakáll et al. 2014). Rogers (1989) estimate that the  
 356 collision rate for an average rain drop in a 55 dBZ rain column is  $\approx 1 \text{ min}^{-1}$ . This would  
 357 imply that rain drops (even in very heavy rainfall) spend an almost negligible fraction of  
 358 time ( $\approx 0.5\%$ ) affected by collision-induced oscillations. Rain drop clustering increases the  
 359 likelihood of these collisions (Jameson and Kostinski 1998). For rain rates of around 10  
 360  $\text{mm hr}^{-1}$  (comparable to those presented in the following case studies), McFarquhar (2004)  
 361 estimate the collision rate to be  $\approx 5 \text{ min}^{-1}$ , implying drops are affected only 3% of the time.  
 362 For very large rain rates ( $100 \text{ mm hr}^{-1}$ ), this fraction increases to 6% as the collision rate  
 363 approximately doubles to  $10 \text{ min}^{-1}$ . Consequently, their impact on  $L$  measurements is likely  
 364 to be small and can be ignored, other than for exceptional rain rates (Thurai et al. 2013).

365 Figure 8 shows how  $L$  varies as a function of  $Z_{DR}$  for gamma distributions with  $\mu = -1$ ,  
 366 0, 2, 4, 8, 12 and 16 computed using Gans theory with the drop shape and oscillation model  
 367 discussed above. Note that lines of constant  $\mu$  diverge with increasing  $Z_{DR}$ . For  $Z_{DR} \gtrsim$

368 0.5 dB, it becomes possible to distinguish  $\mu$ , given the typical error on an  $L$  measurement  
369 (shown in Figure 9).

## 370 7. $\mu$ Retrieval Case Studies

371 We now estimate  $\mu$  using measurements of  $L$  and  $Z_{DR}$  for stratiform rain case studies on  
372 31 January, 25 April and 25 November 2014, and a convective case study on 22 May 2014.  
373 Typical rain rates for each of these case studies can be found in Table 1. Dwells were made  
374 at an elevation angle of  $1.5^\circ$ . Strict data quality filters were applied:  $\text{SNR} > 34$  dB, linear  
375 depolarisation ratio (LDR)  $< -27$  dB (close to the limit of cross-polar isolation) to ensure  
376 no melting particle contamination or ground clutter and range  $> 5$  km to avoid near-field  
377 effects. Theoretical  $L$  and  $Z_{DR}$  were computed using Gans theory using the drop shape and  
378 oscillation model discussed in Section 6 (see Figure 8). Observations were averaged from  
379 10 to 30 s and from range gates of 75 to 300 m to increase the measurement precision of  
380  $L$ . At each gate, the most likely pair of  $\mu$  and  $D_0$  given the observed  $L$  and  $Z_{DR}$  values  
381 was obtained by selecting the closest point in a look-up table of Gamma DSD calculations.  
382 Figure 9a shows the observed  $L$  binned every 0.02 and  $Z_{DR}$  binned every 0.05 dB for the  
383 example of 25 November 2015. Overlaid are lines of constant  $\mu = -1, 0, 2, 4, 8, 12$  and  
384 16. Figure 9b is the same distribution normalised to sum to 1 for each  $Z_{DR}$  bin. The  $f_{hv}^{max}$   
385 on this day was calculated to be 0.9963 (see Section 5d). The observations of  $L$  and  $Z_{DR}$   
386 are generally well contained within the expected range. The median error on  $\hat{L}$  is  $\sigma_L \approx$   
387 0.025, and is shown as a representative error bar in Figure 9. A comparison of these data  
388 with disdrometer measurements from Williams et al. (2014) is included. In this experiment,  
389 the mass spectrum mean diameter ( $D_m$ ) and mass spectrum standard deviation ( $\sigma_m$ ) were  
390 measured using a 2DVD. A  $\sigma_m - D_m$  fit was derived from 18969 1-minute drop spectra  
391 (which can readily be converted to a  $\mu - D_0$  fit). This was in turn used to predict a  $L - Z_{DR}$   
392 relationship, shown by the grey dashed line.  $L$  and  $Z_{DR}$  were also predicted using the

393 proposed  $\mu - \Lambda$  relationship of Cao et al. (2008), also derived from a 2DVD, where:

$$\Lambda = \frac{3.67 + \mu}{D_0} \quad (16)$$

394 This is shown by the black dashed line.

395 The median and inter-quartile range of retrieved  $\mu$  per  $Z_{DR}$  bin for this day is shown in  
396 Figure 10. The median retrieved  $\mu$  is 5 at  $Z_{DR} = 0.8$  dB, increasing to 8 for  $Z_{DR} = 1.6$  dB.  
397 There is significant spread in retrieved  $\mu$  values, containing contributions from measurement  
398 uncertainty on  $L$ , as well as “true ” microphysical variability. The impact of changes in  $L$   
399 on retrieved  $\mu$  is non-linearly related to  $\mu$ ;  $\sigma_L$  contributes more to retrieved  $\mu$  variability  
400 for more monodisperse (higher  $\mu$ ) DSDs, compared to more polydisperse (lower  $\mu$ ) DSDs.  
401 Conversely, the contribution of  $\sigma_L$  to retrieved  $\mu$  variability decreases as  $Z_{DR}$  increases, as  
402 the dual polarisation signature is larger and  $\mu$  is more easily distinguishable (see Figure 8).  
403 To estimate the contribution that the uncertainty on  $L$  measurements makes to this observed  
404 variability,  $\mu$  was retrieved using the median  $L \pm$  the representative uncertainty depicted  
405 in Figure 9. This was then compared to the inter-quartile range of the retrieved  $\mu$  for each  
406  $Z_{DR}$  bin. For  $Z_{DR}$  bins of 0.8, 1, 1.2, 1.4 and 1.6 dB, we estimate that 88%, 66% 32%, 31%  
407 and 27% of the variability respectively can be attributed to  $\sigma_L$ . For  $Z_{DR} > 1$  dB, most of  
408 the variability seen in Figure 10 can be attributed to “true” microphysical variability.

409 Figure 11 shows a comparison with retrieved  $\mu$  for all of the case studies collected. Each  
410 of the dwells in January, April and November were made in stratiform rain, whereas the  
411 May case study contains dwells from convective rain. Overlaid are predicted mean  $\mu$  values  
412 (solid grey) and upper and lower bounds that contain 55% of the measurements (dashed  
413 grey) of Williams et al. (2014) as a function of  $Z_{DR}$  from the disdrometer measurements.  
414 The solid black line shows the predicted  $\mu - Z_{DR}$  using the  $\mu - \Lambda$  relationship of Cao et al.  
415 (2008). There is a large spread in the radar retrieved median  $\mu$  values from case to case.  
416 Each median  $\mu$  estimate is from a very large number of retrieved  $\mu$  estimates, such that the  
417 standard error is smaller than the markers themselves, and so is not shown. The values of

418 retrieved  $\mu$  in January are  $\approx 0$ , close to an exponential DSD for all  $Z_{DR}$  smaller than 1.1 dB.  
419 This is below that predicted by Williams et al. (2014), but agrees well with  $\mu$  predicted by  
420 Cao et al. (2008). Interestingly, the case studies of April and November show  $\mu$  increasing  
421 with  $Z_{DR}$  between 0.5 dB and 1.5 dB, compared to the trend seen by Williams et al. (2014)  
422 and Cao et al. (2008) towards an exponential DSD. The retrieved median  $\mu$  values from  
423 the May case study, although agreeing with the decreasing trend with  $Z_{DR}$ , are significantly  
424 above the Cao et al. (2008) predictions and the upper bound of  $\mu$  from Williams et al. (2014).  
425 Our retrieval suggests that in this case, the rain rate would be overestimated by almost 2  
426 dB if an exponential DSD or the fit of Cao et al. (2008) is assumed. Whereas the  $\mu$  values  
427 are not outside the full range of data measured by Williams et al. (2014), the use of the  
428 proposed  $\mu - D_m$  relationship would cause an overestimate of  $\approx 1$  dB (see Figure 1).

## 429 8. Discussion

430 Our retrievals of  $\mu$  made using  $\rho_{hv}$  and  $Z_{DR}$  are typically larger than the radar estimates  
431 of  $\mu$  of between 1—3 by Thurai et al. (2008) and 0—2 of Illingworth and Caylor (1991).  
432 Perhaps this is not surprising, given that the imperfect co-location of the  $H$  and  $V$  sample  
433 volumes was unaccounted for, and their  $\hat{\rho}_{hv}$  would have been biased low due to averaging  $\rho_{hv}$   
434 rather than  $L$ , both of which are accounted for in our data. Furthermore, Illingworth and  
435 Caylor (1991) do not include drop oscillations in their retrievals, which will have led to a  
436 significant underestimate of  $\mu$ . Whereas there is some agreement of the magnitudes of  $\mu$  for  
437  $Z_{DR} < 1$  dB with predicted Williams et al. (2014) and Cao et al. (2008) values, the apparent  
438 opposite trend towards more monodisperse distributions is consistent among 3 of the 4 case  
439 studies. For the retrieved  $\mu$  to agree with the trend predicted by Williams et al. (2014) or  
440 Cao et al. (2008), a reduction in the drop oscillation amplitudes for smaller drops would be  
441 required so that predicted  $L$  values are higher. However, this would not explain the difference  
442 between the May retrieval results and the predicted  $\mu$  from disdrometer measurements; we

443 estimate that it would require oscillations that are at least an order of magnitude *larger*  
444 to bring these median  $\mu$  estimates into agreement with Williams et al. (2014) or Cao et al.  
445 (2008). An incorrect parameterisation of the drop oscillations alone is unlikely to be able to  
446 account for the disagreement with Williams et al. (2014) and Cao et al. (2008), however, to  
447 better establish the accuracy of the technique, a better quantification of raindrop oscillations  
448 is desirable.

449  $\mu$  estimates derived using radar are sensitive to higher moments of the DSD, whereas  
450 disdrometer estimates tend to use lower moments of the DSD (Cao and Zhang 2009). This  
451 could be partly responsible for the differences between the radar and disdrometer estimated  
452  $\mu$  values. If the DSD shape is not perfectly described by Equation 1, the “effective”  $\mu$  which  
453 is derived may be different even if the underlying DSD shape is the same. It is also possible  
454 that what we have captured is simply natural variability of the DSD in different types of  
455 rainfall (i.e convective and stratiform), and there is not a universal  $\mu - D_0$  relationship. More  
456 case studies are needed to gather a statistical understanding of the behaviour of  $\mu$  using this  
457 retrieval method.

#### 458 *a. Implications for Operational Use of L*

459 Operational radar networks favour the use of rapid scan rates to maximise sample fre-  
460 quency and total sample volume. For UK Met Office radars observing rain with  $1 \text{ ms}^{-1}$   
461 Doppler spectral width, each gate contains  $N_{IQ} \approx 11$  ( $\sigma_L \approx 0.3$ ). Clearly, many more  
462  $N_{IQ}$  are needed than are available for individual gate estimates of  $\mu$ . Greater measurement  
463 precision can be achieved by averaging (with the confidence interval computed using the  
464 aggregated number of independent  $I$  and  $Q$  samples), and assuming  $\mu$  is spatially conserved  
465 over the chosen averaging area. To obtain a  $\mu$  estimate over approximately  $1 \text{ km}^2$ , for ex-  
466 ample, would require the averaging of 2 rays and 10 gates (at a range from the radar of 30  
467 km); this  $L$  estimate would be calculated using  $N_{IQ} = 220$  ( $\sigma_L \approx 0.058$ ). Whereas this may  
468 not be sufficient to distinguish  $\mu$  to as high a resolution as our retrieval (which uses long

dwells and  $N_{IQ} > 1000$ ), this will at least be able to decipher whether  $\mu$  is ‘high’ or ‘low’. Practically, as illustrated in Figure 1, this may be all that is necessary to offer improved rain rate estimates; it is relatively unimportant whether  $\mu$  is 8 or 16, but it is very important to know if it is 0 or 4. Therefore, this method could (with sufficient care to ensure only rain echoes and good SNR) allow for improved rain rates using  $Z$ ,  $Z_{DR}$  and  $L$  compared to only  $Z$  and  $Z_{DR}$ .

For the typical  $\sigma_L$  used in these calculations, we can approximate the error on the retrieved rain rate by considering the contribution of  $\sigma_L$  to the uncertainty in  $\mu$ . For a ‘typical’  $\mu$  of 6, the range of retrieved  $\mu$  is  $\approx \pm 4$ . By referring to Figure 1, we can see that this corresponds to a difference in rain rate of  $\pm 0.5$  dB, or  $\pm 12.5\%$ . The impact of uncertainty in  $\mu$  on rain rate is almost constant for all  $Z_{DR}$  (each of the  $\mu$  lines are approximately parallel in Figure 1 for  $Z_{DR} \gtrsim 0.5$  dB). Therefore, this error will decrease for higher rain rates as the contribution of  $\sigma_L$  to uncertainty in  $\mu$  decreases as a function of  $Z_{DR}$ .

## 9. Conclusions

In this paper, a new variable  $L = -\log_{10}(1 - \rho_{hv})$  is defined that is Gaussian distributed with a width predictable by the number of independent  $I$  and  $Q$  samples, which in turn can be estimated using the Doppler spectral width. This allows, for the first time, the construction of rigorous confidence intervals on each  $\rho_{hv}$  measurement. The predicted errors using this new method were verified using high quality measurements in drizzle from the Chilbolton Advanced Meteorological Radar.

Importantly, the proposed method is of much greater practical use than the linear perturbation error estimation method, as it does not require knowledge of the unknown ‘true’  $\rho_{hv}$  that one is trying to estimate. The method works for both simultaneous or accurately interpolated alternate sampling. However, it does not work for alternate estimators which rely on the Gaussian autocorrelation function to estimate the zero-lag correlation between



494  $H$  and  $V$  pulses (Sachidananda and Zrnica 1989), where  $\rho_{hv}$  estimates can be  $> 1$ .

495 A new technique to account for the imperfect co-location of  $H$  and  $V$  sampling vol-  
496 umes on  $\rho_{hv}$  measurements is presented. The impact of drop oscillations on the observed  $L$   
497 measurements was shown to be significant; omitting oscillations from our Gans simulations  
498 leads to an underestimate of retrieved  $\mu$  of  $\approx 8$ . We further show that failure to use  $L$  over  
499  $\rho_{hv}$  measurements when averaging can lead to a significant bias low in  $\rho_{hv}$  estimates (and  
500 consequently  $\mu$ ), particularly for very short dwell times such as those used operationally.

501 High-precision measurements of  $L$  and  $Z_{DR}$  in rainfall are then used to estimate  $\mu$  in  
502 the gamma DSD for four case studies. We find that our estimates of  $\mu$  in stratiform rain  
503 somewhat agree in magnitude with those from disdrometer studies for small  $Z_{DR}$ , but there  
504 appears to be a tendency to more monodisperse DSDs between  $Z_{DR} = 0.8$  and  $1.5$  dB, unlike  
505 the trend towards an exponential distribution suggested by disdrometer measurements. The  
506 convective case study does display this trend toward lower  $\mu$  as  $Z_{DR}$  increases, but the  
507 magnitude of  $\mu$  remains much larger than predicted by disdrometer measurements. If true,  
508 this would lead to overestimates of retrieved rain rate by  $\approx 1$  dB if the  $\mu - D_m$  relationship of  
509 Williams et al. (2014) is used, or 2 dB if an exponential distribution or the  $\mu - \Lambda$  relationship  
510 of Cao et al. (2008) is used. We find that the  $\mu$  retrieval exhibits sensitivity to the choice of  
511 drop oscillation model. A better understanding of raindrop oscillations would be useful to  
512 fully establish the accuracy of our retrieval technique.

513 The variability in our radar retrieved  $\mu$  could simply be natural variability of the DSD  
514 between convective and stratiform rainfall; there may not be a universal  $\mu - D_0$  relationship.  
515 More case studies are desirable to investigate this further.

516 The  $\mu$  retrieval technique employed here offers improvements over the radar estimates  
517 of Illingworth and Caylor (1991) and Thurai et al. (2008). Illingworth and Caylor (1991)  
518 did not take into account the imperfect co-location of the  $H$  and  $V$  sample volumes on  
519 measurements of  $\rho_{hv}$ , the effect of drop oscillations, or the fact their  $\rho_{hv}$  estimates would  
520 be biased low by averaging short time-series. Each of these effects would cause  $\mu$  to be

521 underestimated. The same is true of Thurai et al. (2008), however drop shapes measured by  
 522 2DVD measurements include oscillations, and so are included in their  $\mu$  estimates.

523 The new error statistics of  $\rho_{hv}$  presented here could aid operational applications that  
 524 require uncertainty on  $\hat{\rho}_{hv}$  to be quantified, or use averages of  $\hat{\rho}_{hv}$ . The use of  $L$  operationally  
 525 to retrieve  $\mu$  is limited by use of rapid scan rates and the corresponding few independent  
 526  $I$  and  $Q$  samples. However, assuming that  $\mu$  is a smoothly varying parameter, averaging  
 527  $L$  could help improve rain rate retrievals; the uncertainty on operationally retrieved rain  
 528 rates using the retrieval technique presented here is estimated to be approximately  $\pm 12.5\%$ .  
 529 Practically, retrieved rain rates are less affected by changes in higher values of  $\mu$  compared  
 530 to changes in lower values. Therefore, operationally, simply being able to distinguish regions  
 531 of ‘high’ and ‘low’  $\mu$  with  $L$  could be sufficient to provide an improvement over existing  
 532  $Z - Z_{DR}$  retrieval techniques.

## 533 APPENDIX

### 534 **The effect of imperfectly co-located H and V samples on $\rho_{hv}$**

535 Consider two measurements of the (complex) amplitudes at horizontal and vertical polar-  
 536 isation  $A_H$  and  $A_V$ . If the two polarisations do not have perfectly matched sample volumes,  
 537 then each amplitude is the sum of (i) a component which is common to both polarisations  
 538  $C_H, C_V$ , (ii) a component which is different for each polarisation  $D_H, D_V$ :

$$A_H = C_H + D_H \tag{A1}$$

539 (and similarly  $A_V = C_V + D_V$ ). The co-polar correlation coefficient is:

$$\rho_{hv} = \frac{\sum A_H A_V^*}{\sqrt{\sum |A_H|^2 \sum |A_V|^2}} \tag{A2}$$

540 where the sums  $\sum$  are taken over many reshufflings of the raindrops. Substituting in the  
 541 expressions for  $A_H$  and  $A_V$  leads to:

$$\rho_{hv} = \frac{\sum C_H C_V^* + \sum D_H C_V^* + \sum C_H D_V^* + \sum D_H D_V^*}{\sqrt{\sum |C_H + D_H|^2 \sum |C_V + D_V|^2}} \quad (\text{A3})$$

542 The first term in the numerator dominates as the number of pulses is increased. This is  
 543 because  $D_H, D_V$ , are uncorrelated with  $C_V, C_H$  (because the reshuffling of particles in the  
 544 different sample volumes is not connected or organised in any way), while  $C_H$  and  $C_V$  are  
 545 highly correlated (because the true  $\rho_{hv}$  is close to 1). The final term is small because  $D_H,$   
 546  $D_V$ , are not correlated (by the same argument), and this term is small in any case since  
 547  $|D| \ll |C|$

548 This leaves us with:

$$\rho_{hv} = \frac{\sum C_H C_V^*}{\sqrt{\sum |C_H + D_H|^2 \sum |C_V + D_V|^2}} \quad (\text{A4})$$

549 In the case of a perfect radar with perfect co-location of the  $H$  and  $V$  samples, then  $D_H, D_V$   
 550 are zero and we get a correlation coefficient which is the true  $\rho_{hv}$  which we are trying to  
 551 obtain (ie setting  $A = C$  in equation A2).

552 In general, for an imperfect radar, we have  $D_H, D_V > 0$  and from the results above we  
 553 see that:

$$\rho_{hv} = \rho_{hv}^{\text{true}} \times f_{hv}^{\text{max}} \quad (\text{A5})$$

554 where

$$f_{hv}^{\text{max}} = \left( \frac{\sum |C_H|^2}{\sum |C_H + D_H|^2} \times \frac{\sum |C_V|^2}{\sum |C_V + D_V|^2} \right)^{1/2} \quad (\text{A6})$$

555 This result is directly analogous to the results of Brangi et al. (1983) on  $\rho_{hv}$  in the presence  
 556 of noise. If we identify  $C$  as our “signal” and  $D$  as our “noise” this equation is identical to  
 557 Equation A1.

558 Crucially, the relationship between the true  $\rho_{hv}$  ( $\rho_{hv}^{\text{true}}$ ) and the one which is actually  
 559 observed is determined simply by how much power (on average over many pulses) comes

560 from the particles which are different for the H and V sample volumes, relative to how much  
561 power comes from the particles which are common to the H and V sample volumes, and that  
562 this factor should be constant for different microphysical situations. Thus if we can measure  
563  $\rho_{hv}$  in drizzle where we know  $\rho_{hv}^{\text{true}} = 1$ , then the measured  $\rho_{hv}$  is simply equal to  $f_{hv}^{\text{max}}$ . This  
564 scaling factor can then be applied to data from all other situations.

## 565 **Acknowledgements**

566 The authors would like to thank the staff at the Chilbolton Facility of Atmospheric and  
567 Radio Research for operation and maintenance of CAMRa, and Chris Walden in particular  
568 for his help with time-series data acquisition. The first author was funded by a National  
569 Environmental Research Council Studentship.

## REFERENCES

- 572 Andrić, J., M. R. Kumjian, D. S. Zrnić, J. M. Straka, and V. M. Melnikov, 2013: Polarimetric  
573 signatures above the melting layer in winter storms: An observational and modeling study.  
574 *Journal of Applied Meteorology and Climatology*, **52 (3)**, 682–700.
- 575 Balakrishnan, N., and D. Zrnic, 1990: Use of polarization to characterize precipitation and  
576 discriminate large hail. *Journal of the atmospheric sciences*, **47 (13)**, 1525–1540.
- 577 Beard, K. V., V. Bringi, and M. Thurai, 2010: A new understanding of raindrop shape.  
578 *Atmospheric Research*, **97 (4)**, 396–415.
- 579 Beard, K. V., and R. J. Kubesh, 1991: Laboratory measurements of small raindrop dis-  
580 tortion. Part 2: Oscillation frequencies and modes. *Journal of the atmospheric sciences*,  
581 **48 (20)**, 2245–2264.
- 582 Brandes, E. A., and K. Ikeda, 2004: Freezing-level estimation with polarimetric radar. *Jour-  
583 nal of Applied Meteorology*, **43 (11)**, 1541–1553.
- 584 Brandes, E. A., G. Zhang, and J. Vivekanandan, 2002: Experiments in rainfall estimation  
585 with a polarimetric radar in a subtropical environment. *Journal of Applied Meteorology*,  
586 **41 (6)**, 674–685.
- 587 Bringi, V. N., and V. Chandrasekar, 2001: *Polarimetric Doppler Weather Radar, Principles  
588 and Applications*. Cambridge University Press, Cambridge, UK.
- 589 Bringi, V. N., T. A. Seliga, and S. M. Cherry, 1983: Statistical properties of the dual-  
590 polarization differential reflectivity ( $Z_{DR}$ ) radar signal. *IEEE Trans. Geosci. Rem Sens.*,  
591 **GE-21 (2)**, 215 –220, doi:10.1109/TGRS.1983.350491.

- 592 Cao, Q., and G. Zhang, 2009: Errors in estimating raindrop size distribution parameters  
593 employing disdrometer and simulated raindrop spectra. *Journal of Applied Meteorology*  
594 *and Climatology*, **48** (2), 406–425.
- 595 Cao, Q., G. Zhang, E. Brandes, T. Schuur, A. Ryzhkov, and K. Ikeda, 2008: Analysis of video  
596 disdrometer and polarimetric radar data to characterize rain microphysics in Oklahoma.  
597 *Journal of Applied Meteorology and Climatology*, **47** (8), 2238–2255.
- 598 Caylor, I. J., 1989: Radar observations of maritime clouds using dual linear polarisation.  
599 Ph.D. thesis, University of Manchester, Manchester, UK.
- 600 Caylor, J., and A. J. Illingworth, 1989: Identification of the bright band and hydromete-  
601 ors using co-polar dual polarization radar. *Preprints, 24th Conf. on Radar Meteorology,*  
602 *Florida, USA, Amer. Meteor. Soc.* 352–357.
- 603 Doviak, R. J., and Zrnica, 2006: *Doppler Radar and Weather Observations*. Dover Publica-  
604 tions, Inc., Mineola, New York, USA.
- 605 Fisher, R. A., 1915: Frequency distribution of the values of the correlation coefficient in  
606 samples from an indefinitely large population. *Biometrika*, **10** (4), 507–521.
- 607 Giangrande, S. E., J. M. Krause, and A. V. Ryzhkov, 2008: Automatic designation of the  
608 melting layer with a polarimetric prototype of the WSR-88D radar. *Journal of Applied*  
609 *Meteorology and Climatology*, **47** (5), 1354–1364.
- 610 Goddard, J., J. D. Eastment, and M. Thurai, 1994: The chilbolton advanced meteorological  
611 radar: A tool for multidisciplinary atmospheric research. *Electronics & communication*  
612 *engineering journal*, **6** (2), 77–86.
- 613 Illingworth, A. J., and I. J. Caylor, 1991: Co-polar correlation measurements of precipitation.  
614 *Preprints, 25th Int. Conf. on Radar Meteorology, Paris, France, Amer. Meteor. Soc.* 650–  
615 653.

616 Jameson, A., 1987: Relations among linear and circular polarization parameters measured  
617 in canted hydrometeors. *Journal of Atmospheric and Oceanic Technology*, **4** (4), 634–646.

618 Jameson, A., and A. Kostinski, 1998: Fluctuation properties of precipitation. Part ii: Re-  
619 consideration of the meaning and measurement of raindrop size distributions. *Journal of*  
620 *the atmospheric sciences*, **55** (2), 283–294.

621 Johnson, R. W., D. V. Kliche, and P. L. Smith, 2014: Maximum likelihood estimation  
622 of gamma parameters for coarsely binned and truncated raindrop size data. *Quarterly*  
623 *Journal of the Royal Meteorological Society*, **140** (681), 1245–1256.

624 Liu, L., V. N. Bringi, V. Chandrasekar, E. A. Mueller, and A. Mudukutore, 1994: Analysis of  
625 the co-polar correlation coefficient between horizontal and vertical polarizations. *Journal*  
626 *of Atmospheric and Oceanic Technology*, **11** (4), 950–963.

627 McFarquhar, G. M., 2004: The effect of raindrop clustering on collision-induced break-up of  
628 raindrops. *Quarterly Journal of the Royal Meteorological Society*, **130** (601), 2169–2190.

629 Papoulis, A., 1965: Probability, random variables, and stochastic processes.

630 Park, H. S., A. V. Ryzhkov, D. Zrnica, and K.-E. Kim, 2009: The hydrometeor classification  
631 algorithm for the polarimetric WSR-88D: Description and application to an mcs. *Weather*  
632 *and Forecasting*, **24** (3), 730–748.

633 Rogers, R., 1989: Raindrop collision rates. *Journal of the Atmospheric Sciences*, **46** (15),  
634 2469–2472.

635 Sachidananda, M., and D. Zrnica, 1989: Efficient processing of alternately polarized radar  
636 signals. *Journal of Atmospheric and Oceanic Technology*, **6** (1), 173–181.

637 Schafer, R., S. Avery, P. May, D. Rajopadhyaya, and C. Williams, 2002: Estimation of  
638 rainfall drop size distributions from dual-frequency wind profiler spectra using deconvolu-

639 tion and a nonlinear least squares fitting technique. *Journal of Atmospheric and Oceanic*  
640 *Technology*, **19** (6), 864–874.

641 Seliga, T., and V. Bringi, 1976: Potential use of radar differential reflectivity measurements  
642 at orthogonal polarizations for measuring precipitation. *Journal of Applied Meteorology*,  
643 **15** (1), 69–76.

644 Szakáll, M., K. Diehl, S. K. Mitra, and S. Borrmann, 2008: A wind tunnel study on the  
645 oscillation of freely falling raindrops. *Proc. Fifth European Conf. on Radar in Meteorology*  
646 *and Hydrology (ERAD 2008)*.

647 Szakáll, M., S. Kessler, K. Diehl, S. K. Mitra, and S. Borrmann, 2014: A wind tunnel study  
648 of the effects of collision processes on the shape and oscillation for moderate-size raindrops.  
649 *Atmospheric Research*, **142**, 67–78.

650 Szakáll, M., S. K. Mitra, K. Diehl, and S. Borrmann, 2010: Shapes and oscillations of falling  
651 raindrops — a review. *Atmospheric Research*, **97** (4), 416–425.

652 Tabary, P., A. Le Henaff, G. Vulpiani, J. Parent-du Châtelet, and J. Gourley, 2006: Melting  
653 layer characterization and identification with a C-band dual-polarization radar: A long-  
654 term analysis. *Proc. Fourth European Radar Conf*, 17–20.

655 Tang, L., J. Zhang, C. Langston, J. Krause, K. Howard, and V. Lakshmanan, 2014: A  
656 physically based precipitation–nonprecipitation radar echo classifier using polarimetric  
657 and environmental data in a real-time national system. *Weather and Forecasting*, **29** (5),  
658 1106–1119.

659 Thurai, M., and V. Bringi, 2005: Drop axis ratios from a 2D video disdrometer. *Journal of*  
660 *Atmospheric & Oceanic Technology*, **22** (7).

661 Thurai, M., D. Hudak, and V. Bringi, 2008: On the possible use of co-polar correlation coeffi-



662 cient for improving the drop size distribution estimates at C band. *Journal of Atmospheric*  
663 *and Oceanic Technology*, **25 (10)**, 1873–1880.

664 Thurai, M., M. Szakáll, V. N. Bringi, and S. K. Mitra, 2013: Collision-induced drop oscilla-  
665 tions from wind-tunnel experiments. *Proc. 36th Conference on Radar Meteorology*.

666 Tokay, A., A. Kruger, and W. F. Krajewski, 2001: Comparison of drop size distribution mea-  
667 surements by impact and optical disdrometers. *Journal of Applied Meteorology*, **40 (11)**,  
668 2083–2097.

669 Torlaschi, E., and Y. Gingras, 2003: Standard deviation of the co-polar correlation coefficient  
670 for simultaneous transmission and reception of vertical and horizontal polarized weather  
671 radar signals. *Journal of Atmospheric and Oceanic Technology*, **20 (5)**, 760–766.

672 Ulbrich, C. W., 1983: Natural variations in the analytical form of the raindrop size distri-  
673 bution. *Journal of Climate and Applied Meteorology*, **22 (10)**, 1764–1775.

674 Unal, C., 2015: High resolution raindrop size distribution retrieval based on the doppler spec-  
675 trum in the case of slant profiling radar. *Journal of Atmospheric and Oceanic Technology*,  
676 **(2015)**.

677 Williams, C. R., 2002: Simultaneous ambient air motion and raindrop size distributions  
678 retrieved from UHF vertical incident profiler observations. *Radio Science*, **37 (2)**, 8–1.

679 Williams, C. R., and Coauthors, 2014: Describing the shape of raindrop size distributions  
680 using uncorrelated raindrop mass spectrum parameters. *Journal of Applied Meteorology*  
681 *and Climatology*, **53 (5)**, 1282–1296.

682 Wilson, D. R., A. J. Illingworth, and T. M. Blackman, 1997: Differential doppler velocity:  
683 A radar parameter for characterizing hydrometeor size distributions. *Journal of Applied*  
684 *Meteorology*, **36 (6)**, 649–663.

685 **List of Tables**

686 1 Typical rain rates ( $R$ ) for each of the case studies, calculated from disdrometer  
687 measurements (April) and radar retrieved  $N_0$ ,  $D_0$  and  $\mu$  values (January, May  
688 and November) 32

TABLE 1. Typical rain rates ( $R$ ) for each of the case studies, calculated from disdrometer measurements (April) and radar retrieved  $N_0$ ,  $D_0$  and  $\mu$  values (January, May and November)

Month	Typical $R$ (mm hr <sup>-1</sup> )	Peak $R$ (mm hr <sup>-1</sup> )
31 January 2014	1–3	8
25 April 2014	2–3	7
22 May 2014	2–7	>30
25 November 2014	2–5	10

## List of Figures

- 689 **List of Figures**
- 690 1 Rain rate (in dB referenced to  $1 \text{ mm hr}^{-1}$ ) per unit radar reflectivity as a  
691 function of  $Z_{DR}$  computed using Gans theory for gamma distributions of  $\mu$   
692 = -1, 0, 2, 4, 8, 12 and 16. The rain rate can vary by as much as 2.5 dB for  
693 a given pair of  $Z$  and  $Z_{DR}$  observations as a result of drop spectrum shape  
694 variability. 36
- 695 2 Example time-series (0.5 s) for single 75 m gates from  $1.5^\circ$  elevation dwells in  
696 (a) drizzle ( $Z_{DR} = 0 \text{ dB}$ ) at 1203 UTC on 6 February 2014, and (b) heavier  
697 rainfall ( $Z_{DR} = 1.1 \text{ dB}$ ) at 1706 UTC on 31 January 2014. For both examples,  
698  $\text{SNR} > 40 \text{ dB}$ . For drizzle, the  $H$  and  $V$  echo time-series vary in unison as the  
699 drops are all spherical. In heavier rainfall, the broader axis ratio distribution  
700 causes the  $H$  and  $V$  time-series to be less correlated. The rate of fluctuation  
701 of the signals is determined by the Doppler spectral width. 37
- 702 3 The frequency distribution of (a)  $\hat{\rho}_{hv}$  calculated from 1159 time-series (0.21 s,  
703 75 m gates) in drizzle ( $Z_{DR} < 0.1 \text{ dB}$ ) and (b)  $\hat{L} = -\log_{10}(1-\hat{\rho}_{hv})$ . The data  
704 was collected at 1203 UTC on 6 February 2014 during a  $1.5^\circ$  elevation dwell  
705 and has very high SNR ( $> 40 \text{ dB}$ ).  $\sigma_v$  for these data ranges between 0.9—1.3  
706  $\text{ms}^{-1}$ . Overplotted on  $\hat{L}$  is a Gaussian curve with same mean and standard  
707 deviation as the measured distribution. 38
- 708 4  $\sigma_L$  as a function of the number of independent  $I$  and  $Q$  samples used to  
709 estimate  $L$  for high SNR measurements in drizzle ( $Z_{DR} < 0.1 \text{ dB}$ ,  $\text{SNR} > 40$   
710  $\text{dB}$ ) at 1203 UTC on 6 February. Different markers correspond to different  
711 Doppler spectral widths. 39

- 712 5 (a) A comparison of the confidence intervals calculated using the new method  
713 and that of Torlaschi and Gingras (2003) in rain ( $\overline{\rho_{hv}} = 0.98$ ) and (b) the  
714 bias introduced by averaging  $\rho_{\hat{h}v}$  instead of  $\hat{L}$ , as a function of  $N_{IQ}$ . For  
715 all  $N_{IQ}$ , the lower confidence interval is higher for the Torlaschi and Gingras  
716 (2003) method, particularly for lower  $N_{IQ}$ , due to the asymmetric nature of  
717 the confidence intervals on  $\rho_{hv}$  using the new method. Averaging  $\rho_{\hat{h}v}$  and not  
718  $\hat{L}$  for small  $N_{IQ}$  can lead to a large bias. 40
- 719 6 (a) Comparison of mean drop axis ratios as a function of equivalent drop  
720 diameter ( $D$ ) from recent experiments of Thurai and Bringi (2005), Szakáll  
721 et al. (2008) and the 4<sup>th</sup> order polynomial fit of older experimental data con-  
722 structed by Brandes et al. (2002). The model of Thurai and Bringi (2005) has  
723 been adapted so that drops are spherical for  $D < 1$  mm. Panels (b)—(d) show  
724 radar and disdrometer  $Z_{DR}$  comparisons calculated using Thurai and Bringi  
725 (2005), Szakáll et al. (2008) and Brandes et al. (2002) from a 5 hour dwell  
726 over a nearby Joss-Waldvogel RD-80 impact disdrometer (approximately 7  
727 km away) in a frontal rain band on 25 April 2014. The time resolution of the  
728 radar measurements was decreased to 30 s to match the integration time of  
729 the disdrometer. At a  $1.5^\circ$  elevation angle, the radar was sampling rain at  
730 a height of  $\approx 183$  m above the disdrometer. The dashed line is a 1:1 line.  
731 The smallest biases are achieved with the Thurai and Bringi (2005) model,  
732 especially for smaller  $Z_{DR}$ , suggesting that these shapes best represent those  
733 of natural rain drops. Therefore, this model is chosen for the analysis. 41
- 734 7 Predicted  $L$  and  $Z_{DR}$  values for gamma distributions of  $\mu = -1$  (solid) and  
735 16 (dashed) with no oscillations (grey), and including oscillations (black).  
736 The inclusion of drop oscillations are crucial to interpretation of  $L$  and  $Z_{DR}$   
737 measurements. The  $f_{hv}^{max}$  is assumed to be 0.9963 to match the case study in  
738 Section 7. 42

- 739 8 Theoretical  $L$  and  $Z_{DR}$  computed using Gans theory for gamma distributions  
740 with  $\mu = -1, 0, 2, 4, 8, 12$  and  $16$ , using Thurai and Bringi (2005) mean drop  
741 axis ratios and oscillation model described in Section 6b. The precision of  $L$   
742 required to estimate  $\mu$  decreases as  $Z_{DR}$  increases. The  $f_{hv}^{max}$  is assumed to  
743 be  $0.9963$  to match the case study in Section 7. 43
- 744 9 (a) 2D PDF of  $L$  and  $Z_{DR}$  observations, and (b) normalised 2D PDF such  
745 that the distribution equals 1 for each  $Z_{DR}$  bin for observations of  $L$  and  $Z_{DR}$   
746 collected from dwells on 25 November 2014.  $L$  is binned over  $0.02$ , and  $Z_{DR}$   
747 every  $0.05$  dB. Overplotted are theoretical  $L$  and  $Z_{DR}$  computed using Gans  
748 theory for gamma distributions of  $\mu = -1, 0, 2, 4, 8, 12$  and  $16$ . Typical  
749 errors on  $L$  and  $Z_{DR}$  are shown as error bars; the error on  $Z_{DR}$  is very small.  
750 The grey dashed line is the predicted  $L$  and  $Z_{DR}$  observations using DSD  
751 parameters from the power-law fit to disdrometer measurements in Williams  
752 et al. (2014). The black dashed line is the predicted  $L$  and  $Z_{DR}$  observations  
753 using the  $\mu - \Lambda$  relationship of Cao et al. (2008). The  $f_{hv}^{max}$  for this day is  
754 measured to be  $0.9963$ . 44
- 755 10 Box plot of retrieved  $\mu$  as a function of  $Z_{DR}$  for  $Z_{DR}$  bins of  $0.2$  dB on 25  
756 November 2014, showing the median and inter-quartile range of the data. 45
- 757 11 Median retrieved  $\mu$  as a function of  $Z_{DR}$  for  $Z_{DR}$  bins of  $0.1$  dB for case  
758 studies of 31 January, 25 April, 22 May and 25 November 2014. The solid line  
759 is the predicted  $\mu$  as a function of  $Z_{DR}$  from the power law fit to disdrometer  
760 measurements of Williams et al. (2014), and  $\sigma_\mu$  corresponds to the upper and  
761 lower bounds that contain 55% of the data. The solid black line shows the  
762 predicted  $\mu - Z_{DR}$  using the  $\mu - \Lambda$  relationship of Cao et al. (2008). 46

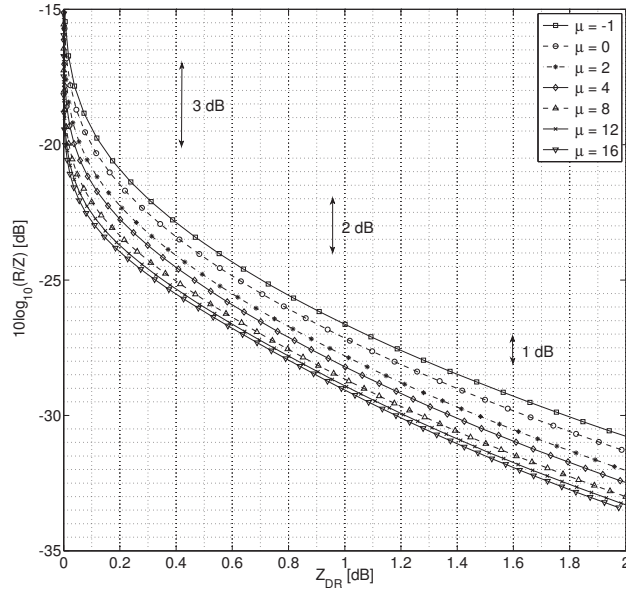


FIG. 1. Rain rate (in dB referenced to  $1 \text{ mm hr}^{-1}$ ) per unit radar reflectivity as a function of  $Z_{DR}$  computed using Gans theory for gamma distributions of  $\mu = -1, 0, 2, 4, 8, 12$  and  $16$ . The rain rate can vary by as much as  $2.5 \text{ dB}$  for a given pair of  $Z$  and  $Z_{DR}$  observations as a result of drop spectrum shape variability.

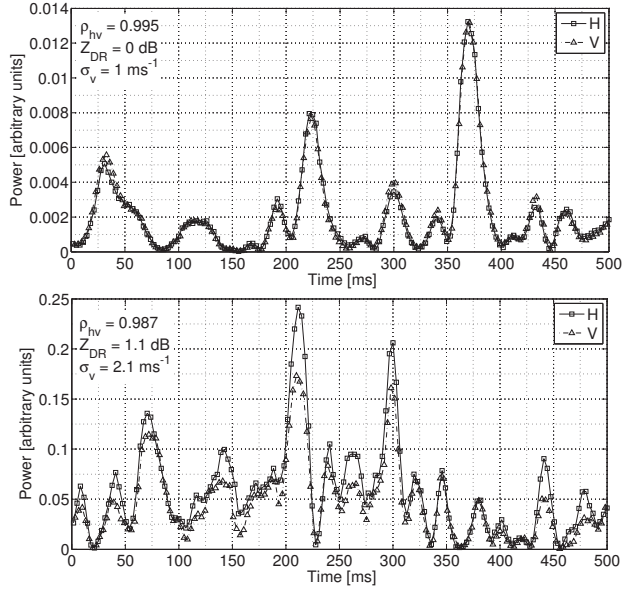


FIG. 2. Example time-series (0.5 s) for single 75 m gates from  $1.5^\circ$  elevation dwells in (a) drizzle ( $Z_{DR} = 0 \text{ dB}$ ) at 1203 UTC on 6 February 2014, and (b) heavier rainfall ( $Z_{DR} = 1.1 \text{ dB}$ ) at 1706 UTC on 31 January 2014. For both examples,  $\text{SNR} > 40 \text{ dB}$ . For drizzle, the  $H$  and  $V$  echo time-series vary in unison as the drops are all spherical. In heavier rainfall, the broader axis ratio distribution causes the  $H$  and  $V$  time-series to be less correlated. The rate of fluctuation of the signals is determined by the Doppler spectral width.



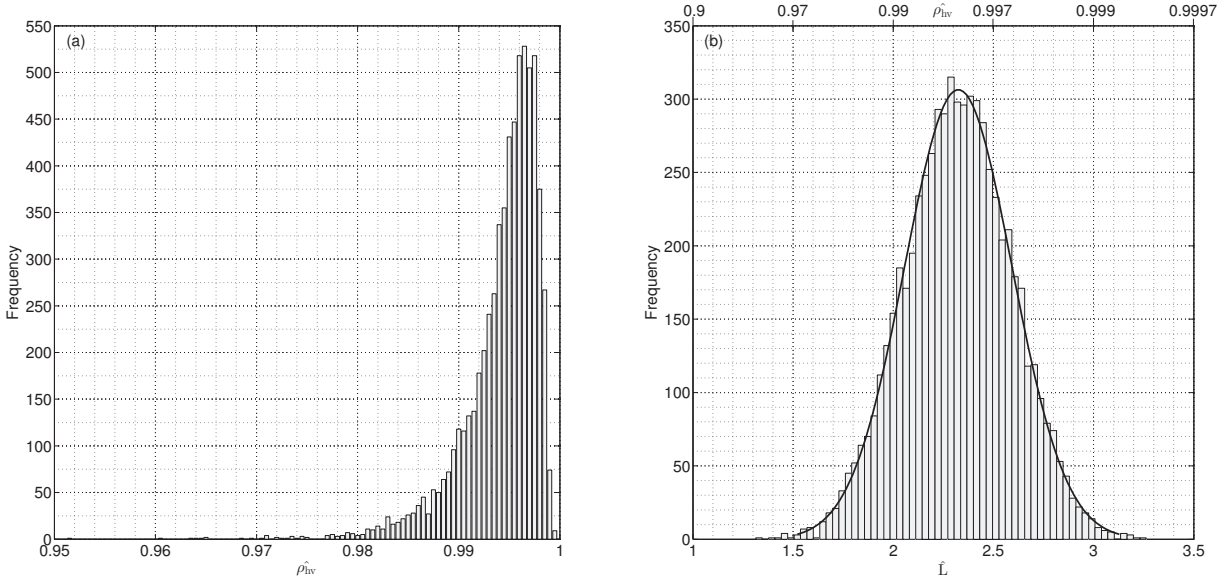


FIG. 3. The frequency distribution of (a)  $\hat{\rho}_{hv}$  calculated from 1159 time-series (0.21 s, 75 m gates) in drizzle ( $Z_{DR} < 0.1$  dB) and (b)  $\hat{L} = -\log_{10}(1-\hat{\rho}_{hv})$ . The data was collected at 1203 UTC on 6 February 2014 during a  $1.5^\circ$  elevation dwell and has very high SNR ( $> 40$  dB).  $\sigma_v$  for these data ranges between  $0.9$ – $1.3$   $\text{ms}^{-1}$ . Overplotted on  $\hat{L}$  is a Gaussian curve with same mean and standard deviation as the measured distribution.

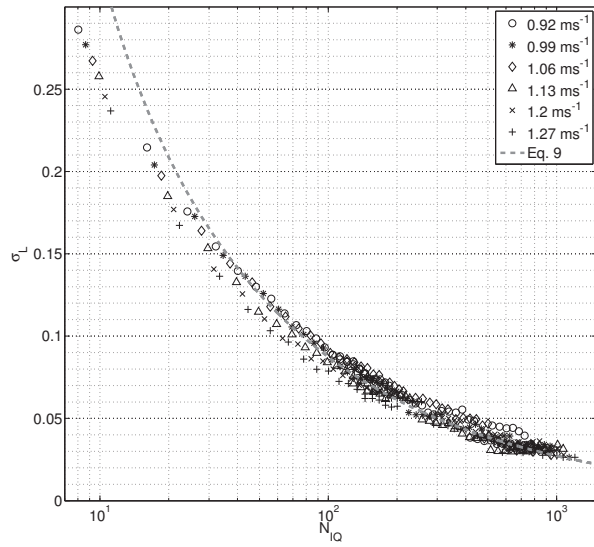


FIG. 4.  $\sigma_L$  as a function of the number of independent  $I$  and  $Q$  samples used to estimate  $L$  for high SNR measurements in drizzle ( $Z_{DR} < 0.1$  dB, SNR  $> 40$  dB) at 1203 UTC on 6 February. Different markers correspond to different Doppler spectral widths.

Rain,  $\overline{\rho_{hv}} = 0.98$

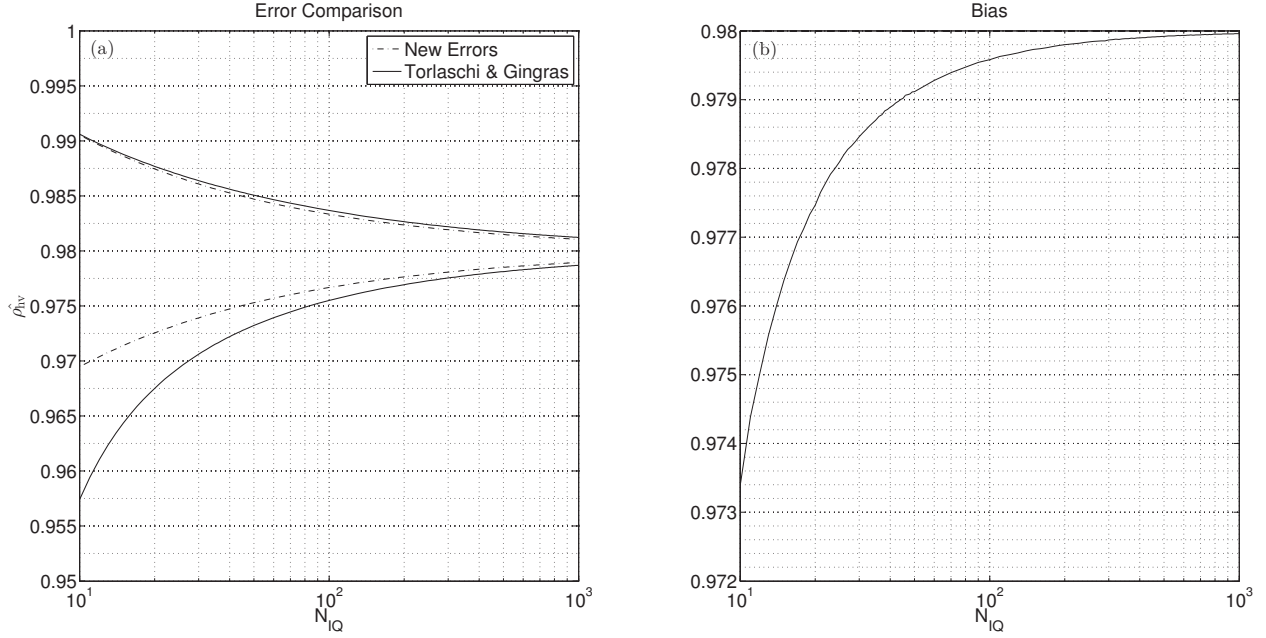


FIG. 5. (a) A comparison of the confidence intervals calculated using the new method and that of Torlaschi and Gingras (2003) in rain ( $\overline{\rho_{hv}} = 0.98$ ) and (b) the bias introduced by averaging  $\hat{\rho}_{hv}$  instead of  $\hat{L}$ , as a function of  $N_{IQ}$ . For all  $N_{IQ}$ , the lower confidence interval is higher for the Torlaschi and Gingras (2003) method, particularly for lower  $N_{IQ}$ , due to the asymmetric nature of the confidence intervals on  $\rho_{hv}$  using the new method. Averaging  $\hat{\rho}_{hv}$  and not  $\hat{L}$  for small  $N_{IQ}$  can lead to a large bias.

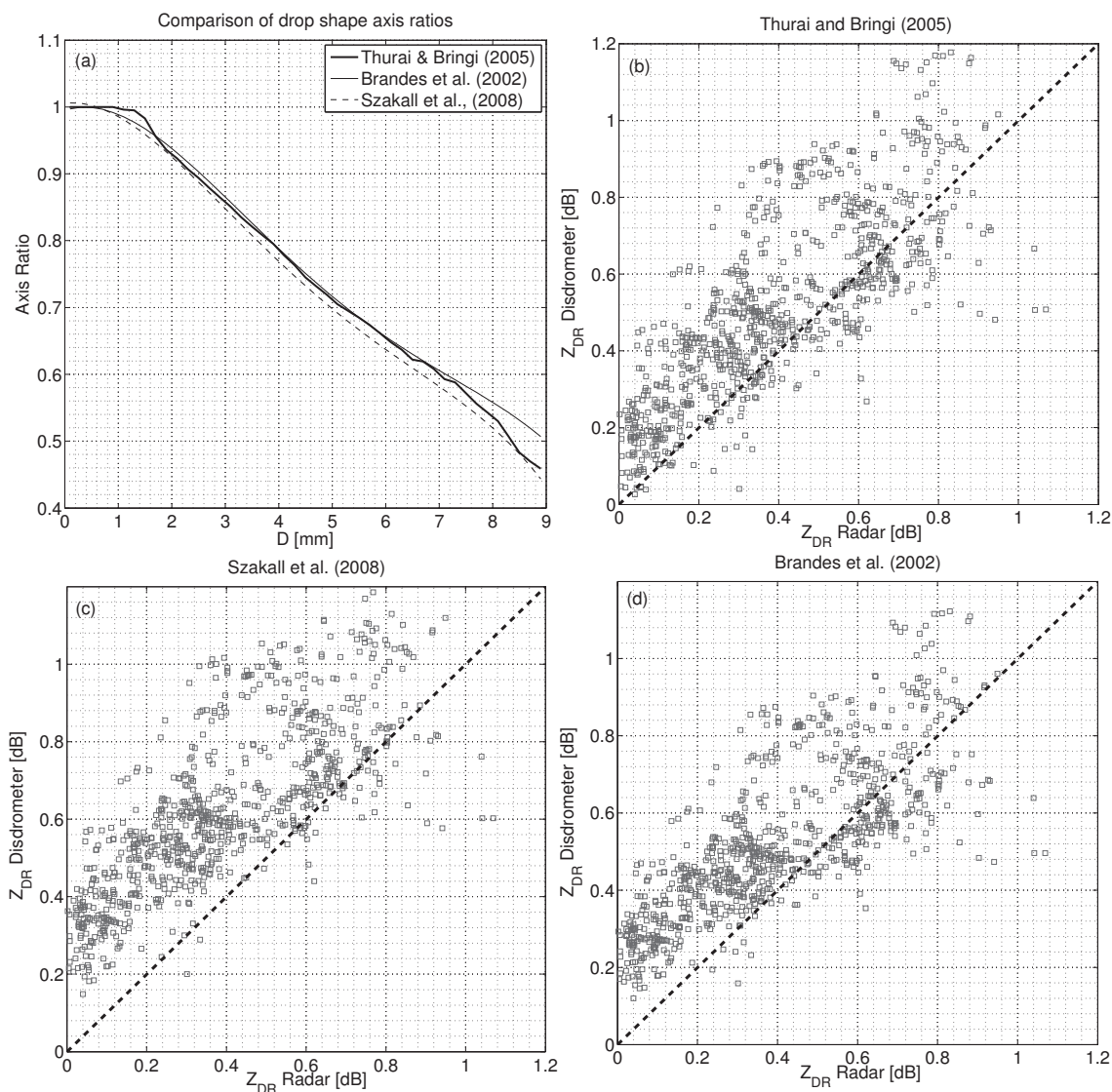


FIG. 6. (a) Comparison of mean drop axis ratios as a function of equivalent drop diameter ( $D$ ) from recent experiments of Thurai and Bringi (2005), Szakáll et al. (2008) and the 4<sup>th</sup> order polynomial fit of older experimental data constructed by Brandes et al. (2002). The model of Thurai and Bringi (2005) has been adapted so that drops are spherical for  $D < 1$  mm. Panels (b)—(d) show radar and disdrometer  $Z_{DR}$  comparisons calculated using Thurai and Bringi (2005), Szakáll et al. (2008) and Brandes et al. (2002) from a 5 hour dwell over a nearby Joss-Waldvogel RD-80 impact disdrometer (approximately 7 km away) in a frontal rain band on 25 April 2014. The time resolution of the radar measurements was decreased to 30 s to match the integration time of the disdrometer. At a  $1.5^\circ$  elevation angle, the radar was sampling rain at a height of  $\approx 183$  m above the disdrometer. The dashed line is a 1:1 line. The smallest biases are achieved with the Thurai and Bringi (2005) model, especially for smaller  $Z_{DR}$ , suggesting that these shapes best represent those of natural rain drops. Therefore, this model is chosen for the analysis.

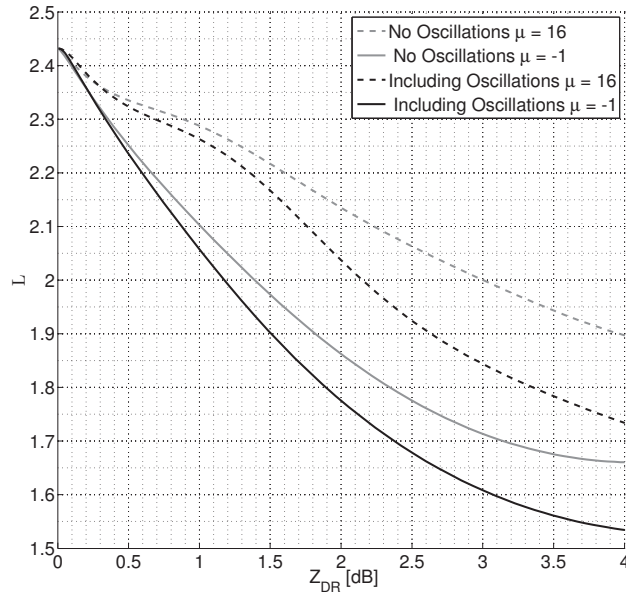


FIG. 7. Predicted  $L$  and  $Z_{DR}$  values for gamma distributions of  $\mu = -1$  (solid) and 16 (dashed) with no oscillations (grey), and including oscillations (black). The inclusion of drop oscillations are crucial to interpretation of  $L$  and  $Z_{DR}$  measurements. The  $f_{hv}^{max}$  is assumed to be 0.9963 to match the case study in Section 7.

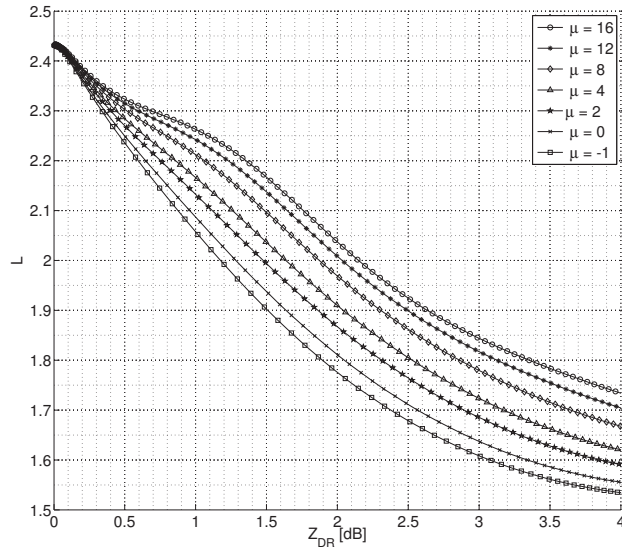


FIG. 8. Theoretical  $L$  and  $Z_{DR}$  computed using Gans theory for gamma distributions with  $\mu = -1, 0, 2, 4, 8, 12$  and  $16$ , using Thurai and Bringi (2005) mean drop axis ratios and oscillation model described in Section 6b. The precision of  $L$  required to estimate  $\mu$  decreases as  $Z_{DR}$  increases. The  $f_{hv}^{max}$  is assumed to be  $0.9963$  to match the case study in Section 7.

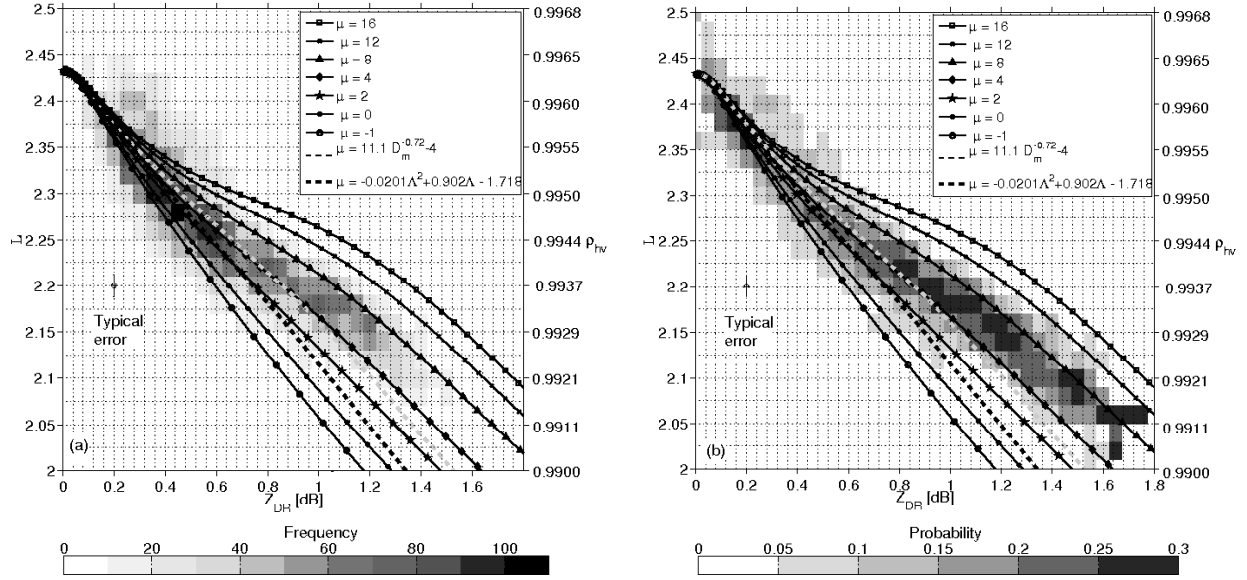


FIG. 9. (a) 2D PDF of  $L$  and  $Z_{DR}$  observations, and (b) normalised 2D PDF such that the distribution equals 1 for each  $Z_{DR}$  bin for observations of  $L$  and  $Z_{DR}$  collected from dwells on 25 November 2014.  $L$  is binned ever 0.02, and  $Z_{DR}$  every 0.05 dB. Overplotted are theoretical  $L$  and  $Z_{DR}$  computed using Gans theory for gamma distributions of  $\mu = -1, 0, 2, 4, 8, 12$  and  $16$ . Typical errors on  $L$  and  $Z_{DR}$  are shown as error bars; the error on  $Z_{DR}$  is very small. The grey dashed line is the predicted  $L$  and  $Z_{DR}$  observations using DSD parameters from the power-law fit to disdrometer measurements in Williams et al. (2014). The black dashed line is the predicted  $L$  and  $Z_{DR}$  observations using the  $\mu - \Lambda$  relationship of Cao et al. (2008). The  $f_{hv}^{max}$  for this day is measured to be 0.9963.

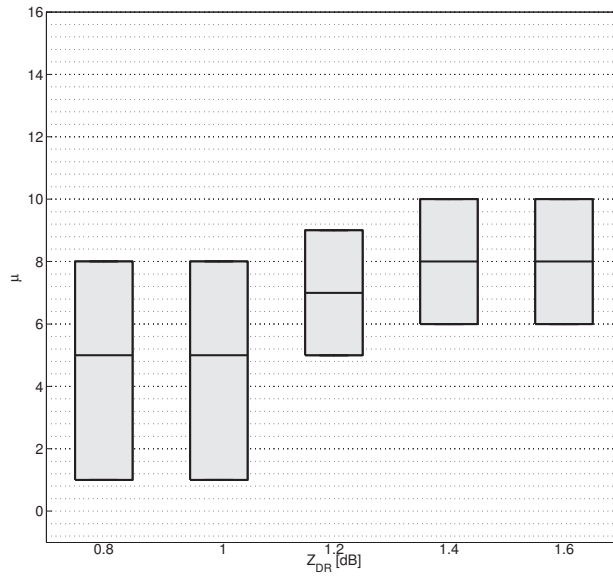


FIG. 10. Box plot of retrieved  $\mu$  as a function of  $Z_{DR}$  for  $Z_{DR}$  bins of 0.2 dB on 25 November 2014, showing the median and inter-quartile range of the data.



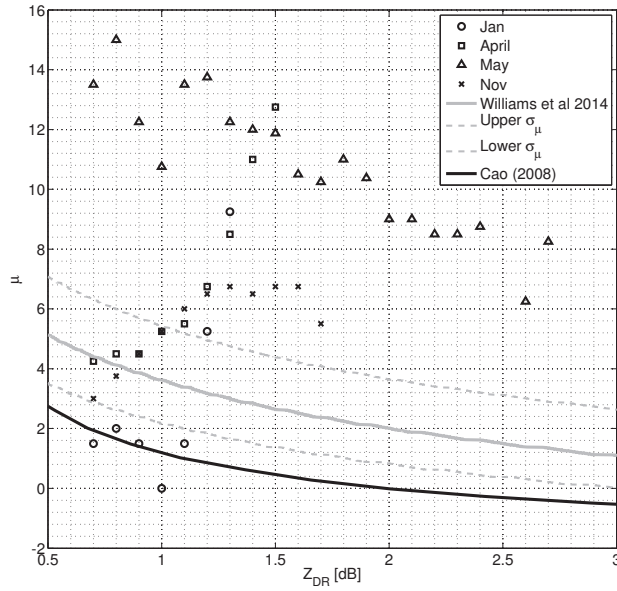


FIG. 11. Median retrieved  $\mu$  as a function of  $Z_{DR}$  for  $Z_{DR}$  bins of 0.1 dB for case studies of 31 January, 25 April, 22 May and 25 November 2014. The solid line is the predicted  $\mu$  as a function of  $Z_{DR}$  from the power law fit to disdrometer measurements of Williams et al. (2014), and  $\sigma_\mu$  corresponds to the upper and lower bounds that contain 55% of the data. The solid black line shows the predicted  $\mu - Z_{DR}$  using the  $\mu - \Lambda$  relationship of Cao et al. (2008).